03,11

Mg_2Ge germanide under pressure: first principle evolutionary search results

© Yu.V. Luniakov

Institute of Automation and Control Processes, Far East Branch, Russian Academy of Sciences, Vladivostok, Russia

E-mail: luniakov@iacp.dvo.ru

Received March 16, 2022
Revised May 19, 2022
Accepted May 20, 2022

The search of optimal structures of magnesium germanide Mg_2Ge under pressure has been performed using the software suite USPEX implementing the evolution algorithm combined with the density functional theory (DFT) approach. It is found that at pressures $P \geq 15$ GPa the triclinic P1 and P-1, monoclinic $P2_1/c$, orthorhombic Amm2 and trigonal P3m1 structures can coexist besides the well-known cubic Fm3m, orthorhombic Pnma and hexagonal $P6_3/mmc$ ones. The new discovered structures are unstable due to potential relief complexity. They transform into orthorhombic Pnma structure at pressures $P < 14$ GPa or hexagonal $P6_3/mmc$ structure at pressures $P > 17$ GPa.

Keywords: Mg_2Ge, crystal structure, phase transitions, hydrostatic pressure, evolutional search, Density Functional Theory.

DOI: 10.21883/PSS.2022.10.54229.316

1. Introduction

Magnesium germanide Mg_2Ge is one of the most studied magnesium compounds of the type Mg_2X (X = Si, Ge and Sn) due to the high melting point $T = 1390$ K [1] and low electrical resistance and thermal conductivity [2–10]. Magnesium compounds Mg_2X are also used in the creation of components for the manufacture of infrared detectors in fiber optics, due to the small width of the energy gap (0.3−0.6 eV) [4]. In addition, magnesium's good ability to hold hydrogen makes Mg_2X compounds very useful for its storage and transportation [11].

Like many oxides and sulfides of rare earth metals, Li_2O, Na_2S, K_2S, Li_2S and Rb_2S, magnesium germanide Mg_2Ge under normal conditions has a simple cubic lattice of antifluorite type of Fm3m symmetry group 225. Even the first experiments performed in 1964 showed that magnesium silicide Mg_2Si with an antifluorite structure is characterized by the following phase transitions under pressure: antifluorite (Fm3m) → anticottunite (Pnma) → hexagonal structure like Ni_2In ($P6_3/mmc$) [12]. In the work [13], calculations were made of the behavior of magnesium compounds Mg_2Ge and Mg_2Sn at a hydrostatic pressure of $0 \leq P \leq 100$ GPa in the generalized gradient approximation (GGA). For the antifluorite → anticottunite phase transition in Mg_2Ge germanide, a pressure of 8.71 GPa was obtained, and for the anticottunite → structure of type Ni_2In it was 33.28 GPa. In 2017 the similar study was performed by the authors [14]. For the transition from antifluorite to anticottunite, they obtained a pressure of 7.85 GPa in GGA and 8.19 GPa in the local electron density (LDA) approximation. For the transition pressure from anticottunite to a Ni_2In type structure in the work [19], the value of 29.77 GPa in the GGA and 63.45 GPa in the LDA was obtained, which differs by more than two times.

Obtaining single-crystal germanide Mg_2Ge under pressure is difficult, since it is a rather brittle material that quickly collapses under pressure. Only relatively recently, the first experimental study of phase transitions in polycrystalline germanide with the stoichiometric composition Mg_2Ge_{1+x} ($x \approx 0.1$) [15] is appeared. X-ray diffraction analysis in the work [15] made it possible to conclude that a composite crystal formed from two incommensurate hexagonal sub-lattices with the same orientation and the same lattice constants a, but with an irrational ratio of the c-period, which leads to the stoichiometry of Mg_2Ge_{1+x}. In an early work of Soviet authors [16], polymorphism in Mg_2Ge germanide under pressure up to $P = 10$ GPa was proposed based on X-ray diffraction data. In a later work [15] Russian scientists abandoned the idea of polymorphism in favor of the idea of a composite crystal consisting of at least two incommensurate atomic subsystems. In the work of Chinese scientists [17], studies of the temperature dependence of conductivity and the Hall coefficient at different pressures were carried out. The change in the nature of this dependence indicated a change in the nature of conductivity from semiconductor one to metallic one at pressures of $7.4 < P \leq 7.8$ GPa, as well as during phase transitions from antifluorite to anticottunite ($P = 9.5$ GPa) and from anticottunite to structure of type Ni_2In ($P = 35.6$ GPa). This work is devoted to simulating of phase transitions in crystalline germanide Mg_2Ge using the methods of evolutionary search for optimal structures in the pressure range sufficient to observe the listed phase transitions. Application of evolutionary search to other magnesium compounds made it possible to reproduce known phase transitions and

obtain unknown structures of Mg_2Si silicide with C2/m, Cmmm and Pmmm symmetry [18]. This gives a hope to expect new results for magnesium germanide Mg_2Ge.

2. Calculation procedure

To determine the optimal structures with the lowest enthalpy, modern evolutionary search methods were used, implemented in the Universal Structure Predictor software package: Evolutionary Xtallography (USPEX) [19–22]. In the process of evolutionary search, more than 20 generations of various structures were generated, depending on the convergence: 24 structures in each, except for the first generation (140 structures). In the first generation, structures were generated randomly with arbitrary space symmetry. In subsequent generations, 60% of the structures of the previous generation with the lowest enthalpy were used, of which 70% were generated using the inheritance operator, and 30% were generated as a result of applying the lattice mutation operator. Convergence was considered achieved if the most energy-favorable structure was maintained for 20 generations. The optimization of the geometry for the obtained structures was performed using the conjugate gradient method implemented in the VASP [23] program with accuracy in energy of ~ 0.1 meV per cell. The cutoff energy of the plane-wave basis in this case was $E_{\text{cut}} = 520$ eV for ease of comparison with the Material Project database www.materialsproject.org [24]. The exchange-correlation potential was chosen in the Purdue–Burke–Ernzerhof parametrization [25] in the generalized gradient approximation (GGA). For numerical integration in the process of evolutionary search, the density of k-points was set equal to $2\pi \cdot 0.05\,\text{Å}^{-1}$. For enthalpy calculations, the following definition at zero temperature was used: $F = E + P \cdot V$, where E is total energy, P is external pressure, V is primitive cell volume. The external hydrostatic pressure was chosen in the range of $0 \le P \le 30$ GPa, sufficient to reproduce all known phase transitions in germanide Mg_2Ge.

3. Results and discussion

Table 1 lists the most energetically favorable structures for pressures $0 \le P \le 30$ GPa in decreasing order of enthalpy.

For each pressure, the row number in Table 1 is proportional to the value of the enthalpy plotted relative to the lowest enthalpy for that pressure. We see that, under normal conditions, the most energetically favorable turns out the orthorhombic structure Amm2 of the space group of symmetry 38. At the same time, it is known that under normal conditions, Mg_2Ge germanide, like Mg_2Si silicide and Mg_2Sn stannide, has a simple cubic structure Fm3m of space symmetry 225. Determination of symmetry using the FINDSYM [26] utility with an accuracy of allowable displacement of atoms within $0.02\,\text{Å} \le \sigma \le 0.2\,\text{Å}$ also identifies the structure obtained under normal conditions as Fm3m. With increase in the accuracy of the allowable displacement of atoms to $\sigma \le 0.01$ Å the symmetry can be determined as a lower: groups from 21 (C222) to 38 (Amm2). If to compare the enthalpy of the resulting structure Amm2 and the cubic structure Fm3m № 408 from the Material Project database [24], then their differences are less than 0.5 meV per formula unit Mg_2Ge over the entire pressure range $0 \le P \le 30$ GPa, which makes these structures almost indistinguishable. The lattice constant for the Amm2 structure practically coincides with the lattice constant of the cubic structure № 408 from the database [24] up to the second decimal place after the separator of the integer and fractional parts.

Table 1. Symmetry of optimal structures for various pressures plotted against the most energetically favorable structure at each pressure

Enthalpy, eV	Pressure, GPa						
	~ 0	5	10	15	20	25	30
1.4	–	2	14	–	–	–	1
1.3	–	–	62	62	–	–	–
1.2	–	–	–	–	35	–	–
1.1	–	–	–	–	–	–	–
1.0	–	–	2	–	–	–	–
0.9	–	–	62	–	–	–	–
0.8	–	–	–	–	–	–	62
0.7	–	62	–	–	–	156	–
0.6	–	–	–	–	–	–	–
0.5	–	63	–	–	–	–	–
0.4	–	–	–	–	–	–	–
0.3	–	–	–	–	–	–	–
0.2	–	–	–	–	–	–	–
0.1	–	–	–	–	–	–	164
0.0	38	1	2	14	62	156	1

As we see in Table 1, under a pressure of 5 GPa, the triclinic crystal structure of the smallest symmetry P1 is optimal. Depending on the given precision, the FINDSYM utility [26] determines its structure as a trigonal P-1 space group 2 ($\sigma \le 0.002$) or an anticottunite type structure Pnma of space groups 62 ($\sigma \ge 0.1$). Under a pressure of 10 GPa, the monoclinic structure $P2_1/c$ of the symmetry group 14 is already optimal, which can be defined as the structure of the symmetry group 11 with a decrease in the allowable displacement of atoms σ to 0.005 Å, or as a structure of the symmetry group 62 as the parameter σ increases to 0.01 Å. Space groups 2, 11 and 14 are subgroups of group 62, while group 2 is a subgroup of both group 11 and 14. The relationship between the structures of symmetry groups 2, 11, 14, 62 and 194, defined as a result of using the structural analysis utilities https://www.cryst.ehu.es/cryst/rel.html [27], is illustrated in Tables 2 and 3.

The first line of Table 2 shows the coordinates of the basic atoms of the initial orthorhombic Pnma structure, obtained

Table 2. Displacement of basic atoms in Mg_2Ge cells with symmetry reduction $194 \to 62 \to 11 \to 2$

Lattice parameters	Structure	Atom	Coordinates		
$a = 4.24$ Å $b = 7.344$ Å $c = 5.361$ Å	194 ($\to 62$)	Mg1(4c) Mg2(4c) Ge1(4c)	1/4 1/4 3/4	$1/4 - y_1$ 5/12 11/12	z_1 $3/4 + z_2$ $1/4 + z_3$
$a = 3.912$–3.924 Å $b = 7.476$–7.518 Å $c = 6.123$–6.244 Å	62 ($\to 11$)	Mg11(2i) Mg12(2i) Mg21(2i) Mg22(2i) Ge1(2i) Ge2(2i)	1/4 1/4 1/4 1/4 1/4 1/4	$1/2 + y_1$ $1 - y_1$ $1/6 + y_2$ $1/3 - y_2$ $2/3 - y_3$ $5/6 + y_3$	$1/6 - z_1$ $2/3 - z_1$ z_2 z_2 $1/2 + z_3$ $1/4 - z_3$
$a = 3.912$–3.924 Å $b = 7.476$–7.518 Å	11	Mg11(2i) Mg12(2i)	1/4 1/4	$1/2 + y1 + u1$ $1/2 + y1 + u1$	$1/6 - z1$ $1/6 - z3$
$a = 3.912$–3.924 Å $b = 7.46$–7.518 Å $c = 6.123$–6.244 Å	11 ($\to 2$)	Mg11(2i) Mg12(2i) Mg21(2i) Mg22(2i) Ge1(2i) Ge2(2i)	1/4 1/4 1/4 1/4 1/4 1/4	$1/2 + y1 + u1$ $1 - y1 + u1$ $1/6 + y2 + u2$ $1/3 - y2 + u2$ $2/3 - y_3$ $5/6 + y3$	$1/6 - z1$ $2/3 - z1$ z2 z2 $1/2 + z3$ $1/4 - z3$

Table 3. Displacement of basic atoms in Mg_2Ge cells with symmetry reduction $194 \to 62 \to 14 \to 2$

Lattice parameters	Structure	Atom	Coordinates		
3.9 Å$\leq a \leq$ 4.7 Å	194 ($\to 62$)	Mg1(4c) Mg2(4c) Ge1(4c)	1/4 1/4 3/4	$1/4 - y_1$ 5/12 11/12	z_1 $3/4 - z_2$ $1/4 + z_3$
5.4 Å$\leq b \leq$ 7.1 Å	62 ($\to 14$)	Mg1(4e) Mg2(4e) Ge1(4e)	$1/4 - u_1$ $1/4 + u_2$ 3/4	$1/4 - y1$ 5/12 11/12	z_1 $3/4 - z_2$ $1/4 + z_3$
4.1 Å$\leq c \leq$ 4.3 Å	14 ($\to 2$)	Mg11(2i) Mg12(2i) Mg21(2i) Mg22(2i) Ge1(2i) Ge2(2i)	$1/4 - u_1 + v_1$ $-1/4 - u_1 + v_1$ $1/4 + u_2$ $-1/4 - u_2$ $-1/4 - v_2$ $1/4 - v_2$	$1/4 + y_1$ $1/4 - y_1$ $1/12 - y_2$ $-5/12 - y_2$ $-3/12 - y_2$ $1/8 - y_1$	z_1 $1/2 - z_1$ $z_2 - 3/4$ $1/4 - z_2$ $1/4 + z_3$ $1/4 - z_3$

as a result of the displacement of atoms from highly symmetric positions in the hexagonal structure of higher symmetry $P6_3/mmc$ in the (010) and (001) directions. In Table 2 these displacements are denoted as y_1, z_1, z_2 and z_3. When the $62 \to 11$ symmetry is reduced, the $Mg_{21,22}$ and $Ge_{1,2}$ atoms are displaced by $y_{2,3}$ along the (010) direction in the coordinate system of the monoclinic group 11. The reduction of $11 \to 2$ symmetry occurs due to the subsequent displacement of Mg atoms by $u_{1,2}$ along the (010) direction. As for the $62 \to 14$ symmetry reduction, as shown in Table 3, it occurs due to the displacement of magnesium atoms by $u_{1,2}$ along the (100) direction in the coordinate system of the monoclinic group 14. The subsequent $14 \to 2$ symmetry reduction can occur due to the displacement of atoms by $v_{1,2}$ along the (100) direction and by $y_{2,3}$ along the (010) direction.

From Table 1, we see that at a sufficiently high pressure $P = 25$ GPa, the structure with P3m1 symmetry of the group 156 becomes the most energetically favorable. This symmetry can be defined as 194, 12 and 2 depending on the given accuracy of the allowable displacement of atoms in the range 0.001 Å$\leq \sigma \leq$ 0.01 Å. Since the monoclinic structure C2/m of the symmetry group 12 is a subgroup of the group 194, it can be obtained as a result of displacement of the basic atoms in the $P6_3/mmc$ structure along the (100) and (001) directions. When the displacement of atoms also occurs in the third direction (010), then the symmetry is already lowered to group 2 (P-1), and we see in Table 1 this structure as the most favorable under pressure $P = 10$ GPa.

Each of the structures in Table 1, obtained as a result of evolutionary search, was re-optimized after symmetry redefinition by the FINDSYM utility [26] with higher accuracy in

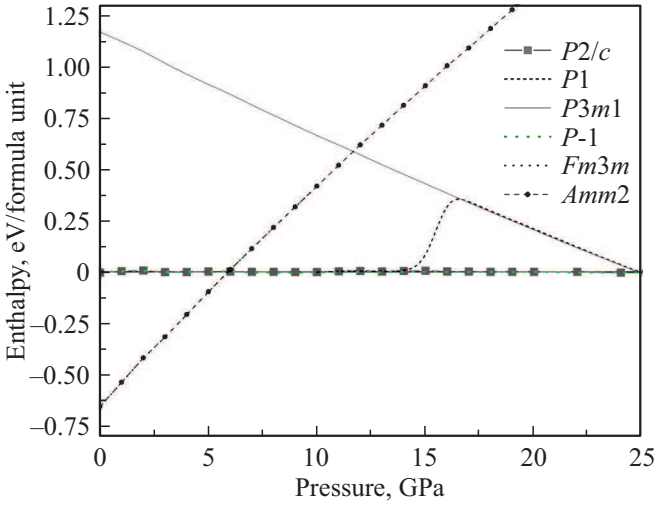

Figure 1. The enthalpy of various obtained structures as a function of pressure, plotted relative to the orthorhombic Pnma structure, chosen as a reference.

allowable displacement σ. Figure 1 shows the dependence of enthalpy on pressure obtained as a result of a number of such calculations, plotted with respect to the orthorhombic Pnma structure of the symmetry group 62 chosen as a standard. In addition to the structures calculated in this way, for comparison, the enthalpy of antifluorite structures № 408 and structures of the Ni_2In type № 1018794 from the database [24] was also calculated depending on pressure. The difference in enthalpy for structures of close symmetry is within the accuracy of these calculations. For example, for structures 11 and 2, the enthalpy differs by less than 2.5 meV per formula unit, for 1 and 62 differs by less than 1.25 meV, for 14 and 62 differs by less than 0.25 meV, for 2 and 62 differs by less than 0.75 meV. The enthalpy of the trigonal structure P3m1 of the symmetry group 156 practically coincides with the enthalpy of the hexagonal structure $P6_3/mmc$ № 1018794 from the database [24], which indicates their indistinguishability in the experiment.

The most energetically favorable under normal conditions is the orthorhombic structure Amm2 of symmetry group 38. Its energy is practically the same as the energy for the well-known cubic structure № 408 of symmetry group 225 taken from the database [24]. When performing independent calculations of the structure № 408, the difference in energy with the orthorhombic structure Amm2 is no more than 0.1 meV per formula unit. For the lattice constant, the difference between the Amm2 structure obtained in these calculations and the structure № 408 is no more than 0.01 Å in the pressure range $0 \leq P \leq 20$ GPa, or less than 0.2%.

The enthalpy curve of a simple cubic structure intersects with the enthalpy curve of the orthorhombic structure of the symmetry group at the point 5.88 GPa, indicating a transition from the antifluorite structure to the anticottunite structure Fm3m → Pnma. As a result of this phase transition, the first order derivative discontinuity of the thermodynamic potential (i.e. of the volume) is occurs as shown in Fig. 1, indicating to the first order phase transition, It can be seen from Fig. 4 in the work [13] that the reduction in volume as a result of the phase transition Fm3m → Pnma at a pressure of $P = 8.71$ GPa is also about 4 Å^3, which practically coincides in absolute value with the results obtained in this work. The relative volume change in this case is equal to 6.82% [13]. As for other theoretical results, in the work [14] at the transition pressure from antifluorite Fm3m to anticottunite Pnma $P = 7.85$ GPa, the relative volume change is 12.3%. This discrepancy may be due to different values of the obtained transition pressures Fm3m → Pnma. In the work [14] it is 7.85 GPa, in the work [13] is 8.71 GPa, in this work is 5.88 GPa. Since at different pressures there will be different initial and final values of the volumes of the cubic and orthorhombic cells, the relative change in volume will also be different.

The measurement of the dependence for the resistance of Mg_2Ge germanide on temperature in the work [17] showed that under a pressure of $P = 7.4$ GPa, the semiconductor → metal (metallization) transition occurs, and at a pressure of 8.7 GPa, a phase transition occurs from the Fm3m antifluorite structure to the Pnma anticottunite structure. To study the metallization processes, calculations were made of the density of electronic states in the antifluorite structure, which are shown in Fig. 2. As the pressure increases, the upper occupied states begin to be superimposed on the Fermi level (E_{Fermi}) and at pressures $P \geq 8$ GPa we can already observe the metallization of Mg_2Ge, which agrees with the experimental data [17], in which metallization was observed at pressures $P \approx 7.4$ GPa.

The pressure dependence of the lattice cell volume per one formula unit is shown in Fig. 3. For a cubic structure Fm3m, the lattice cell volume decreases from 66 to 58 Å^3 as the pressure increases to 8.7 GPa. In the

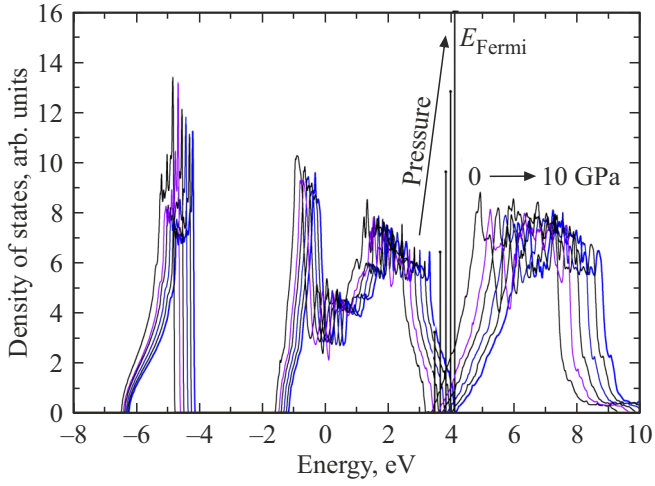

Figure 2. Density of electronic states of Mg_2Ge structure of antifluorite under pressure from 0 to 10 GPa. As the pressure increases, the EFermi level and upper occupied states shift to the right.

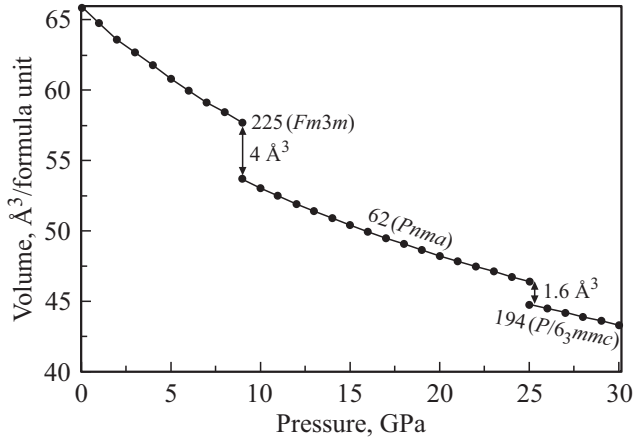

Figure 3. Lattice cell volume of various Mg_2Ge structures depending on pressure.

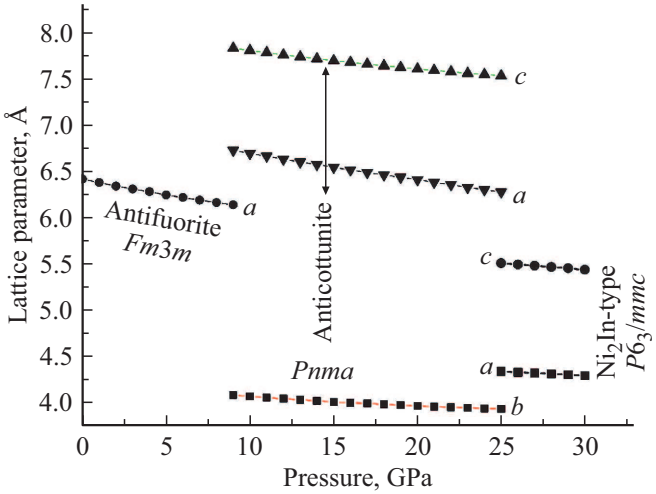

Figure 4. Structural parameters of different lattice cells of Mg_2Ge with cubic, hexagonal and orthorhombic structure depending on pressure.

work [13] in Fig. 4 one can observe the corresponding reduction in volume from about 64 to 56 Å^3 as the pressure increases from 0 to 8 GPa. For the orthorhombic Pnma structure, as the pressure increases from 9 to 25 GPa, the volume decreases from 53.7 to 46.4 Å^3, or by 13.6%. In the work [13] the same volume in the corresponding pressure range decreases from 51.7 to 43.8 Å^3, as can be seen from Fig. 4. In the work [14] in LDA, the corresponding volume decreases from approximately 54 to 47 Å^3. For the hexagonal structure $P6_3/mmc$, the lattice cell volume decreases from 51.7 to 43.3 Å^3 as the pressure increases from 9 to 30 GPa, or by 16.2%. In the work [13] at a pressure of 33 GPa, the volume of a hexagonal cell is 41.5 Å^3 (Fig. 4 of lattice cell in the article [13]), which also agrees with the obtained values.

As for the lattice parameters, their changes with increasing pressure are shown in Fig. 4. For a simple cubic cell Fm3m, the lattice constant a changes in the range from 6.4 to 6.1 Å as the pressure increases from 0 to 9 GPa, which agrees with the data of the work [13] (Fig. 4), where a decreases from 6.35 to 6.0 Å. For the orthorhombic cell Pnma, parameter a decreases from 6.72 to 6.27 Å, parameter b decreases from 4.08 to 3.93 Å, and parameter c decreases from 7.83 to 7.53 Å for $9 \le P \le 25$ GPa, which also agrees with the results [13], where $6.2\,\text{Å} \le a \le 6.7\,\text{Å}$, $3.7\,\text{Å} \le b < 3.8\,\text{Å}$ and $7.5\,\text{Å} \le c \le 7.8\,\text{Å}$ for $9\,\text{GPa} \le P \le 25\,\text{GPa}$. In the work [14] for the symmetry Pnma cell at $P = 7.85$ GPa, one obtain slightly higher values of the lattice parameters: $a = 7.08$ Å, $b = 4.25$ Å, $c = 8.21$ Å. For a hexagonal structure of type Ni_2In, the parameter a varies from 4.33 to 4.29 Å, and the parameter c varies from 5.50 to 5.43 Å at $25\,\text{GPa} \le P \le 30\,\text{GPa}$. This is in good agreement with the results of calculations [13] $a \approx 4.04$ Å and $c \approx 5.24$ Å at $P = 33.28$ GPa. As for the work [14], we can only compare the data at a fixed pressure corresponding to the normal conditions $P = 0$ and the transition of Pnma → $P6_3/mmc$ $P = 29.77$ GPa. Under normal conditions $P = 0$ in work [14] it turns out $a \approx 4.73$ Å, $c \approx 6.15$ Å in comparison with the given results $a \approx 4.73$ Å, $c \approx 6.10$ Å. For $P \approx 30$ GPa these values are $a \approx 4.37$ Å and $c \approx 5.55$ Å [14] compared to the obtained values of $a = 4.29$ Å and $c = 5.43$ Å. Changes in the lattice cell volume with an increase in pressure from 0 to 30 GPa are approximately the same, as far as can be judged from the figures in the article [14].

In Fig. 1 under pressure $P \approx 15.5$ GPa we can observe a phase transition without volume change, corresponding to the so-called symmetry increase P1 → $P6_3/mmc$. This transition is an artifact of the calculation, and during the subsequent optimization of the orthorhombic structure $P6_3/mmc$, the inverse transition $P6_3/mmc$ → P1 is not observed. Instead, a reversible $P6_3/mmc$ → Pnma transition is observed at a pressure of 24.81 GPa, which can be seen in Fig. 1 at the point of intersection of the P3m1 curve with the abscissa axis corresponding to the reference Pnma structure. The resulting phase transition is a first-order phase transition, since it occurs with a discontinuity in the first order derivative of the thermodynamic potential, i.e. the volume. In this work, the change in volume is 1.63 Å^3, or 3.5%, while in other calculations it is obtained in the range from 3.12% [13] to 12.29% [14]. For the second phase transition Pnma → $P6_3/mmc$, different calculations give very different pressure values: in the work [13] is 18.4 GPa, in the work [14] is 29.77 GPa, while in this work it is equal to 24.81 GPa. It can be noted that for the Pnma → $P6_3/mmc$ phase transition in LDA, compared to GGA, the value of 63.45 GPa was obtained in [14], which is much beyond the spread of the values of the phase transition pressure Pnma → $P6_3/mmc$ in GGA in different calculations. As for the experimental value of the phase transition pressure Pnma → $P6_3/mmc$, in the work [17] it is 33.3 GPa, which is 8.5 GPa (25.5%) exceeds the value obtained in this work. For the Fm3m → Pnma phase transition, the experiment [17] also gives a value

of 8.7 GPa overestimated by 48% compared to the results in this work $P = 5.88$ GPa. In other calculations [14], smaller values of the transition pressure Fm3m → Pnma $P = 7.85$ GPa are also obtained, while in the work [13] it is the value $P = 8.71$ GPa practically coincides with the experiment [17]. Such discrepancies can be associated both with the complexity of the potential relief in orthorhombic and hexagonal structures (see Fig. 1), and with the inevitable experimental error, in which it is difficult to uniformly distribute pressure throughout the polycrystalline sample. The complexity of the potential relief leads to the complexity of the germanide structure, which is consistent with the earlier work of Russian scientists [15,16]. It is rather problematic to calculate the incommensurate structures described in [15] by evolutionary methods, since this requires large computational costs and does not guarantee results.

4. Conclusion

The results of evolutionary search reliably reproduce the known phase transitions in Mg_2Ge germanide under pressure (antifluorite (Fm3m) → anticottunite (Pnma) → Ni_2In ($P6_3/mmc$)) and make it possible to predict new crystal structures: triclinic P1 and P-1, monoclinic $P2_1/c$, orthorhombic Amm2 and trigonal P3m1, which can exist in a wide pressure range of 6−25 GPa. These structures are unstable due to the complex potential relief and can transform into more stable orthorhombic Pnma or hexagonal $P6_3/mmc$ depending on the pressure. The instability of the structures of crystalline Mg_2Ge complicates their experimental study and may explain the difficulties in the practical production of Mg_2Ge germanide under pressure.

Funding

The work was supported by the state budget of the IACP FEB RAS (theme No. 0202-2021-0002).

The calculations were carried out using the equipment of the Shared Resource Center „Far Eastern Computing Resource“ IACP FEB RAS (https://cc.dvo.ru).

Conflict of interest

The author declares that he has no conflict of interest.

References

[1] A.A. Nayeb-Hashemi, J.B. Clark. Bulletin Alloy Phase Diagrams **5**, 466 (1984).
[2] H. Udono, H. Tajima, M. Uchikoshi, M. Itakura. Jpn. J. Appl. Phys. **54**, *7S2*, 07JB06 (2015).
[3] A. Vantomme, J.E. Mahan, G.L. James, P.B. Margriet, V. Bael, K. Temst, C.V. Haesendonck. Appl. Phys. Lett. **70**, *9*, 1086 (1997).
[4] H. Zhang, X. Zhong, J.C. Shaw, L. Liu, Y. Huang, X. Duan. Energy Environ Sci. **6**, *9*, 2621 (2013).
[5] Y. Liao, M. Fan, Q. Xie, Q. Xiao, J. Xie, H. Yu, S. Wang, X. Ma. Appl. Surf. Sci. **458**, 360 (2018).
[6] J. Tani, H. Kido. Physica B **364**, *1−4*, 218 (2005).
[7] J. Tani, M. Takahashi, H. Kido. J. Alloys. Compd. **485**, 764 (2009).
[8] M. Cahana, Y. Gelbstein. Intermetallics **120**, *5*, 106767 (2020).
[9] G. Murtaza, A. Sajid, M. Rizwan, Y. Takagiwa, H. Khachai, M. Jibran, R. Khenata, S. Bin Omran. Mater. Sci. Semicond. Proc. **40**, 429 (2015).
[10] G. Castillo-Hernandez, M. Yasseri, B. Klobes, S. Ayachi, E. Müller, J. Boor. J. Alloys. Compd. **845**, 156205 (2020).
[11] L. Schlapbach, A. Züttel. Nature **414**, *686*1, 353 (2001).
[12] P. Cannon, E.T. Conlin. Science **145**, *3631*, 487 (1964).
[13] F. Yu, J.-X. Sun, T.-H. Chen. Physica B **406**, *9*, 1789 (2011).
[14] M. Guezlane, H. Baaziz, Z. Charifi, A. Belgacem-Bouzida, Y. Djaballah. J. Sci. Adv. Mater. Devices **2**, *1*, 105 (2017).
[15] N.B. Bolotina, T.I. Dyuzheva, N.A. Bendeliani, V. Petricek, A.E. Petrova, V.I. Simonov. J. Alloys. Compd. **278**, *1−2*, 29 (1998).
[16] T.I. Dyuzheva, S.S. Kabalkina, L.F. Vereshchagin. DAN SSSR **228**, *5*, 1073 (1976) (in Russian).
[17] Y. Li, Y. Gao, Y. Han, C. Liu, C. Peng, Q. Wang, F. Ke, Y. Ma, C. Gao. Appl. Phys. Lett. **107**, *14*, 142103 (2015).
[18] Yu.V. Lunyakov. FTT **62**, *5*, 783 (2020) (in Russian).
[19] C.W. Glass, A.R. Oganov, N. Hansen. Comp. Phys. Commun. **175**, *11−12*, 713 (2006).
[20] A.O. Lyakhov, A.R. Oganov, H.T. Stokes, Q. Zhu. Comp. Phys. Commun. **184**, *4*, 1172 (2013).
[21] A.R. Oganov, Y.M. Ma, Y. Xu, I. Errea, A. Bergara, A.O. Lyakhov. Proc. Natl. Acad. Sci. **107**, 7646 (2010).
[22] A.R. Oganov, A.O. Lyakhov, M. Valle. Acc. Chem. Res. **44**, *3*, 227 (2011).
[23] G. Kresse, J. Furthmuller. Phys. Rev. B **54**, *16*, 11169 (1996).
[24] A. Jain, Sh. Ping Ong, G. Hautier, Wei Chen, W.D. Richards, S. Dacek, Sh. Cholia, D. Gunter, D. Skinner, G. Ceder, K.A. Persson. APL Materials **1**, *1*, 011002 (2013).
[25] J.P. Perdew, K. Burke, M. Ernzerhof. Phys. Rev. Lett. **77**, *18*, 3865 (1996).
[26] H.T. Stokes, D. Hatch. J. Appl. Cryst. **38**, *1*, 237 (2005).
[27] G. de la Flor, D. Orobengoa, E. Tasci, J.M. Perez-Mato, M.I. Aroyo. J. Appl. Cryst. **49**, *Part 2*, 653 (2016).